HHS Public Access

Author manuscript

Mol Imaging Biol. Author manuscript; available in PMC 2022 April 01.

Published in final edited form as:

Mol Imaging Biol. 2021 April ; 23(2): 230–240. doi:10.1007/s11307-020-01557-x.

The Roles of ZnT1 and ZnT4 in Glucose-Stimulated Zinc Secretion in Prostate Epithelial Cells

Su-Tang Lo[1,2], **Daniel Parrott**[1,2], **M. Veronica Clavijo Jordan**[1,2,3], **Diya Binoy Joseph**[3], **Douglas Strand**[3], **U-Ging Lo**[4], **Ho Lin**[5], **Anza Darehshouri**[6], **A. Dean Sherry**[*,1,2,7]

[1]Advanced Imaging Research Center, UT Southwestern Medical Center, Dallas, Texas, 150390-8568, United States

[2]Department of Radiology, UT Southwestern Medical Center, Dallas, Texas, 150390-8896, United States

[3]Athinoula A. Martinos Center for Biomedical Imaging, Massachusetts General Hospital, Harvard Medical School, Charlestown, Massachusetts, 02129, United States

[4]Department of Urology, UT Southwestern Medical Center, Dallas, Texas, 150390-9110, United States

[5]Department of Life Sciences, National Chung Hsing University, Taichung City, 402 Taiwan

[6]Electron Microscopy Core Facility, UT Southwestern Medical Center, Dallas, Texas, TX 150390-9039, United States

[7]Department of Chemistry, University of Texas at Dallas, Richardson, Texas, 150083, United States

Abstract

Purpose—We have previously demonstrated by MRI that high glucose stimulates efflux of zinc ions from the prostate. To our knowledge, this phenomena had not been reported previously and the mechanism remains unknown. Here, we report some initial observations that provide new insights into zinc processing during glucose stimulated zinc secretion (GSZS) in the immortalized human prostate epithelial cell line, PNT1A. Additionally, we identified the subtypes of zinc-containing cells in human benign prostatic hyperplasia (BPH) tissue to further identify which cell types are likely responsible for zinc release *in vivo*.

Procedure—An intracellular fluorescence marker, FluoZin-1-AM, was used to assess the different roles of ZnT1 and ZnT4 in zinc homeostasis in wild type (WT) and mRNA knock-down

*Corresponding Author: A. Dean Sherry, PhD, Advanced Imaging Research Center, The University of Texas Southwestern Medical Center, 5323 Harry Hines Blvd, NE 4.210, Dallas, Texas 150390-8568, Phone: (214) 645-2730, dean.sherry@utsouthwestern.edu.

Potential conflict of interest

A.D.S. is a co-founder of VitalQuan, LLC, which is developing MRI and fluorescence sensors for detecting Zn^{2+} in tissues.

PNT1A cell lines. Additionally, Bafilomycin A1 (Baf) was used to disrupt lysosomes and assess the role of lysosomal storage during GSZS. ZIMIR, an extracellular zinc-responsive fluorescent marker, was used to assess dynamic zinc efflux of WT and ZnT1 mRNA knock-down cells exposed to high glucose. Electron microscopy was used to assess intracellular zinc storage in response to high glucose, and evaluate how Bafilomycin A1 affects zinc traficking. BPH cells were harvested from transurtheral prostatectomy tissue and stained with fluorescent zinc granule indicator (ZIGIR), an intracellular zinc-responsive fluorescent marker, before being sorted for cell types using flow cytometry.

Results—Fluorescent studies demonstrate that ZnT1 is the major zinc efflux transporter in prostate epithelial cells and that loss of ZnT1 via mRNA knockdown combined with lysosomal storage disruption results in a nearly 4-fold increase in cytosolic zinc. Knockdown of ZnT1 dramatically reduces zinc efflux during GSZS. Electron microscopy (EM) reveals that glucose stimulation significantly increases lysosomal storage of zinc; disruption of lysosomes via Baf or ZnT4 mRNA knockdown increases multi-vesicular body (MVB) formation and cytosolic zinc levels. In human BPH tissue, only the luminal epithelial cells contained significant amounts of zinc storage granules.

Conclusions—Exposure of prostate epithelial cells to high glucose alters zinc homeostasis by inducing efflux of zinc ions via ZnT1 channels and increasing lysosomal storage via ZnT4. Given that prostate cancer cells undergo profound metabolic changes that results in reduced levels of total zinc, understanding the complex interplay between glucose exposure and zinc homeostasis in the prostate may provide new insights into the development of prostate carcinogenesis.

Keywords

prostate metabolism; glucose stimulated zinc secretion; prostate zinc efflux; intracellular zinc storage; ZnT1 expression; zinc-responsive contrast agents; prostate zinc homeostasis; ZnT1 mediated efflux; lysosomal zinc storage; PNT1A

1. Introduction

Citrate accumulates to high levels in the prostate due to partial inhibition of the citric acid cycle enzyme, aconitase-2 (ACO-2), by high concentrations of Zn^{2+} ions [1,2,3]. This allows the prostate to transfer excess citrate and Zn^{2+} ions into prostatic fluid where they serve as an energy source for sperm (citrate) and to enhance sperm motility (Zn^{2+}), both crucial for male fertility [4,5]. To maintain these vital functions, the prostate must acculate and maintain large amounts of Zn^{2+}, approximately 1 mg zinc per gram of wet prostate tissue [4,6,7]. However, high concentrations of Zn^{2+} can also be toxic to cells causing oxidative damage due to inhibition of glutathione reductase. Thus, prostate cells must fine tune Zn^{2+} levels by sequestration of excess Zn^{2+} in storage granules in order to maintain a carefully balanced Zn^{2+} homeostasis [8,9].

Zinc homeostasis is a complex process involving the interplay of two major families of zinc transporters. The SLC39A family, otherwise known as the ZIP family, generally governs cellular zinc influx [4, 10]. In prostate cells, ZIP1 resides in the plasma membrane and is the dominant zinc influx transporter [4, 10, 11, 12]. The SLC30A family, otherwise known as

the ZnT family, generally govern zinc efflux. The major zinc efflux channel, ZnT1, resides in the plasma membrane and is ubiquitously expressed throughout the human body [10, 14]. Numerous studies have demonstrated that excess zinc ions in cellular growth media increases expression of ZnT1 and thereby the capacity of efflux zinc ions [9, 14]. Gene silencing by shRNA-targeted ZnT1 expression results in increased apoptosis and decreased cell viability [15] while storage of excess Zn^{2+} ions in granules for eventual lysosomal exocytosis is governed by ZnT4 transporters [9, 10, 13]. Loss of this function through shRNA silencing of ZnT4 leads to decreased zinc efflux and increased apoptosis, demonstrating the importance of lysosomal storage in maintaining zinc homeostasis and cell viability [15].

In prostate cancer, down-regulation of ZIP1 and up-regulation of ZnT4 results in an approximately 6-fold decrease in intracellular zinc levels compared to normal prostate [6, 12, 16, 17]. This suggests that zinc levels in prostate tissue may serve as a biomarker for progression of prostate cancer. Previously, a zinc-responsive magnetic resonance imaging (MRI) contrast agent was used to detect secretion of Zn^{2+} ions from the mouse prostate in healthy animals and loss of Zn^{2+} secretion from sections of the prostate in transgenic adenocarcinoma TRAMP mice as they developed cancer [18]. Interestingly, zinc release from the mouse prostate was detected only after a bolus of glucose was administered to fasted animals. Given that the MRI contrast agent used in those experiments is thought to be impermeable to cell membranes, the MRI signal enhancement was assumed to reflect Zn^{2+} movement from intracellular stores into extracellular spaces initiated by a sudden increase in plasma glucose. To our knowledge, stimulation of zinc secretion from the prostate by specific secretagogues had not been reported previously and the molecular mechanism of this connection remains largely unknown. Given that zinc plays such an important role in overall prostate function and health, unravelling details about the connection between an increase in plasma glucose and zinc efflux from the prostate may lead to new insights into the progression of prostate cancer. Here, we investigated the redistribution of Zn^{2+} ions in prostate epithelial cells after switching from low to high glucose levels can results in net transport of Zn^{2+} from cells. These new results offer some insights into the connection between Zn^{2+} homoeostasis and glucose metabolism in the prostate.

2. Results

2.1 Distinct roles of ZnT1 and ZnT4 in modulating intracellular levels of Zn^{2+}

We previously reported that exposure of prostate epithelial cells, PNT1A, to high concentrations of glucose results in efflux of Zn^{2+} ions into the cell media [18]. However, those experiments did not identify which pools of mobile Zn^{2+} ions (cytosolic, mitochondrial, lysosomal, or granular) contribute to this phenomenon, now referred to as glucose stimulated zinc secretion (GSZS). Mobile Zn^{2+} pools that contribute to zinc homeostasis have been previously identified in HeLa cells using a combination of FluoZin1-AM, an intracellular zinc-responsive probe, and LysoTracker® Red DND-99 (Thermo), a dye that localizes to lysosomes [9]. To our knowledge, these pools have not been identified in this manner in prostate epithelial cells. Accordingly, PNT1A cells were cultured in RMPI-1640 media supplemented with 150 μM $ZnSO_4$ in ensure that enough Zn^{2+} was

available to fill all possible storage pools. 24 hours prior to imaging, PNT1A cells were either treated with 20 nM Baf, a small molecule that disrupts lysosomal structures by inhibiting H^+-ATPase [19] or vehicle alone (DMSO) as a control. After 24 hours, cells were removed from the culture media and loaded with FluoZin-1-AM and LysoTracker® Red DND-99 (Thermo) for 30 minutes. A Zeiss 780 confocal microscope was used for cell imaging. Merged fluorescent FluoZin-1-AM and LysoTracker images demonstrate significant co-localization of both fluorescent probes indicating that lysosomes are important in compartmental storage of zinc ions (Fig. 1c). Cells treated with Baf displayed significantly lower LysoTracker® signals than cells treated with DMSO indicating disrupted lysosomes (Figs. 1b and e). Without the lysosomes serving as zinc storage sites, cytoplasmic zinc increased as indicated by the increased FluoZin-1-AM signal (FluoZin-1-$AM_{\text{intensity density}}$ DMSO: ~$1.16 \pm 0.21 \times 10^7$; Baf: ~$2.41 \pm 0.45 \times 10^7$, $p < 0.0001$) (Fig. 1s), and merged signal intensity disappeared (Fig 1f). Interestingly, when lysosomes were disrupted, intracellular Zn^{2+} ions appeared to accumulate in alternative intracellular compartments (white arrows in Fig. 1d).

Since we observed only mildly elevated cytoplasmic Zn^{2+} in Baf-treated WT cells, this suggested that some of the excess Zn^{2+} originating from disrupted lysosomal pools may have been exported from cells using the zinc exporter, ZnT1, located in the outer cell membrane [14, 15]. To test this hypothesis, a lentivirus was used to generate a stable ZnT1-impaired PNT1A cell line (PNT1A-shZnT1) and the same experiments were performed on the ZnT1-impaired cell line (Fig. 1g-l). Western Blot analyses were used to confirm the absence of ZnT1 in the impaired cell line (Fig. S1). Treatment with DMSO resulted in only a slight increase in the signal of FluoZin-1-AM in PNT1A-shZnT1 cells compared to wild type cells (PNT1A-WT)(FluoZin-1-$AM_{\text{intensity}}$ in WT_{DMSO}: $1.16 \pm 0.21 \times 10^7$; FluoZin-1-$AM_{\text{intensity}}$ in $shZnT1_{DMSO}$: $1.33 \pm 0.26 \times 10^7$; $p = 0.01$) (Fig. 1s). In contrast, treatment with Baf induced a significant increase in cytoplasmic Zn^{2+} in PNT1A-shZnT1 cells compared to the PNT1A-WT (FluoZin-1-$AM_{\text{intensity}}$ in $shZnT1_{Baf}$: $4.65 \pm 1.73 \times 10^7$ vs. WT_{Baf}: $2.41 \pm 0.45 \times 10^7$; $p < 0.0001$) (Fig. 1s). This indicates that the loss of both lysosomal storage and zinc efflux via ZnT1 significantly reduces the ability of cells to modulate cytoplasmic zinc levels. Interestingly, an enhanced FluoZin-1-AM signal was also observed in other compartments in Baf-treated PNT1A-shZnT1 cells (white arrows in Fig. 1j), similar to that seen in Baf treated PNT1A-WT cells (Fig. 1d).

To examine the role that ZnT4 plays in intracellular zinc storage, a second lentivirus was used to generate a stable ZnT4-impaired PNT1A cell line (PNT1A-shZnT4). Western Blots confirmed the reduced amount of ZnT4 in the impaired cells (Fig. S1). Cells were cultured overnight with 150 μM $ZnSO_4$ and 20 nM Baf or DMSO, and then co-loaded with FluoZin-1-AM and LysoTracker®. In cells exposed only to DMSO, there was a mild, but significant decrease in the FluoZin-1-AM signal in PNT1A-shZnT4 cells compared to PNT1A-WT (FluoZin-1-$AM_{\text{intensity density}}$ $shZnT4_{DMSO}$: $0.86 \pm 0.04 \times 10^7$; FluoZin-1-$AM_{\text{intensity density}}$ WT_{DMSO} : $1.16 \pm 0.21 \times 10^7$, $p < 0.0001$), consistent with lower intracellular Zn^{2+} (Fig. 1s). PNT1A-shZnT4 cells cultured with Baf displayed a significantly reduced FluoZin-1AM signal compared to shZnT1 cells (FluoZin-1-$AM_{\text{intensity density}}$ $shZnT1_{Baf}$: $4.65 \pm 1.73 \times 10^7$ vs. FluoZin-1-$AM_{\text{intensity density}}$ $shZnT4_{Baf}$: $1.52 \pm 0.05 \times 10^7$, $p < 0.0001$), indicating that despite the reduction in intracellular Zn^{2+} storage capabilities,

PNT1A-shZnT4 cells were still able to efflux extracellular zinc via ZnT1. An enhanced FluoZin-1-AM signal was again observed in other compartments in Baf-treated cells (Fig. 1p) compared to DMSO treated cells (Fig. 1m).

2.2 High glucose enhances storage of liposomal zinc

During the tissue culture, PNT1A-WT cells displayed tolerance in culture condition under high $ZnSO_4$ concentration up to 0.5 mM. To examine whether exposure to high glucose results in more storage of lysosomal Zn^{2+}, PNT1A-WT cells were cultured for 72 hours with 300 μM $ZnSO_4$ to enhance the lysosomal zinc storage and then challenged with low (3 mM) or high (18 mM) glucose for 15 minutes. PNT1A-WT cells grown in the absence of $ZnSO_4$ was used as control. The storage of Zn^{2+} in lysosomes were evaluated by transmission electron microscopy (TEM)(Fig. 2). In cells grown without 300 μM of $ZnSO_4$, no electron dense granules were observed regardless of glucose concentration. With zinc supplementation, large electron-rich granules with an average diameter of 1.4 ± 0.5 μm (n = 23) were detected in cells exposed to high glucose (18 mM) whereas cells treated with low glucose (3 mM) had significantly smaller granules (average diameter: 0.6 ± 0.1 μm; n = 16) ($p < 0.0001$). This indicates that high glucose promotes storage of lysosomal Zn^{2+} may be a mechanism to prevent zinc toxicity in prostate cells.

2.3 Lysosomal impairment leads to multi-vesicular body storage of zinc ions

The previous fluorescence experiments demonstrate that disruption of lysosomal acidification by Baf leads to increased cytosolic Zn^{2+}, particularly when ZnT1 efflux is concurrently impaired. Interestingly, Zn^{2+} appeared to accumulate in other intracellular compartments after treatment with Baf. To understand how intracellular Zn^{2+} storage changes at a subcellular level, TEM experiments were conducted on Baf-treated PNT1A-WT, PNT1A-shZnT1, and PNT1A-shZnT4 cells. Initially, the cells were supplemented with 300 μM of $ZnSO_4$ to compare the TEM study as shown in Figure 2. However, both PNT1A-shZnT1 and PNT1A-shZnT4 cells were unable to survive under such condition. Thus, cells were cultured for 24 hours in RPMI-1640 media supplemented with 150 μM $ZnSO_4$, as well as either 20 nM Baf or DMSO (Figure 3). In each of the cell lines treated with Baf, large multi-vesicular bodies (MVBs), categorized as late endosomes that can either later merge with lysosomes or directly fuse with the plasma membrane, were apparent (Fig. 3b, d, and f). The appearance of MVBs reflects a roadblock along the endosomal-lysosomal pathway [20, 21] (**Scheme**, Fig. 3) The number and density of the MVBs was highest in the PNT1A-shZnT1 cells (24 MVBs in a representative PNT1A-shZnT1 cells versus 11 MVBs in a representative PNT1A-WT cells) consistent with an increase in cytosolic Zn^{2+} (as detected by FluoZin-1-AM) and a reduced ability to efflux Zn^{2+}. In DMSO treated PNT1A-shZnT4 cells, the number of lysosomes were similar in number in comparison to PNT1A-WT cells but were 65% less dense compared to those in PNT1A-WT cells, consistent with the requirement of ZnT4 for loading Zn^{2+} into lysosomes (Fig. 3a and e). In PNT1A-shZnT4 cells treated with Baf, the number and density of MVBs were similar to those in PNT1A-WT cells (12 in a representative PNT1A-shZnT4 cell versus 11 in a PNT1A-WT cell) (Fig. 3f).

2.4 The role of ZnT1 in glucose-stimulated zinc secretion

The loss of ZnT1 in PNT1A-shZnT1 cells resulted in increased cytoplasmic Zn^{2+} when lysosomal zinc storage was concurrently disrupted. This highlights the crucial role of ZnT1 in modulating a rise in cytosolic Zn^{2+}. To investigate the role that ZnT1 plays in dynamic Zn^{2+} efflux in response to glucose stimulation, two live cell fluorescent imaging experiments were conducted on PNT1A-WT and PNT1A-shZnT1 cells. First, FluoZin-1-AM was used to monitor intracellular zinc levels after glucose stimulation in real time and, second, the Zn^{2+}-sensitive fluorescent indicator, ZIMIR, was used to monitor efflux of Zn^{2+} from cells. ZIMIR, an extracellular fluorescent probe ($K_{D(Zn)}$ ~ 0.45 μM) designed to anchor into the outer plasma membrane of cells has been successfully used to monitor Zn^{2+} co-secreted with insulin from MIN6 insulinoma cell lines and from isolated mouse pancreatic islets in response to glucose [18, 22].

PNT1A-WT and PNT1A-shZnT1 cells were cultured in RPMI-1640 supplemented with 150 μM $ZnSO_4$ for 72 hr prior to *in vitro* fluorescence imaging. After removing the $ZnSO_4$-supplemented culture medium, cells were then exposed to 1 μM ZIMIR or FluoZin-1-AM for 30 minutes in secretion assay buffer (SAB) buffer, a physiologic salt solution containing 3 mM glucose. After collecting a baseline fluorescence image, the glucose concentration was increased to 18 mM. PNT1A-WT cells displayed a rapid increase (over 2 min) in the signals of both FluoZin-1-AM signal (Fig. 4a) and ZIMIR (Fig. 4b) after exposure to 18 mM glucose. This demonstrates that both intracellular and extracellular Zn^{2+} increase in response to high glucose. In PNT1A-shZnT1 cells, neither intracellular extracellular Zn^{2+} increased after exposure to high glucose. The higher background signal of FluoZin-1-AM in PNT1A-shZNT1 cells compared to PNT1A-WT cells indicates that cytosolic Zn^{2+} was initially higher in those cells compared to PNT1A-WT cells. Therefore, switching to 18 mM glucose had little further impact on cytosolic Zn^{2+} levels. These experiments do verify the importance of ZnT1 in export of Zn^{2+} when exposed to high glucose.

2.5 Distribution of zinc by cellular sub-types in human benign prostatic hyperplasia (BPH) tissue

Our results demonstrate how zinc transporters manage the intracellular distribution of zinc ions in prostate epithelial cells. In vivo, there are multiple different epithelial subtypes, including basal and luminal, and the previous GSZS observed MRI results do not distinguish between possible subtypes of cells that may be responsible for release of Zn^{2+} ions. To evaluate the distribution of zinc granules as a function of cell subtype, human prostate tissue samples were obtained under institutional review board (IRB) guidelines from BPH patients undergoing a simple prostatectomy. The tissue was first exposed to collagenase to separate out individual cells and the resulting cells were stained with antibodies to CD326 (to mark all epithelial cells) and CD26 (to mark only luminal epithelial cells) [31, 32, 33]. The cells were incubated with ZIGIR, an intracellular fluorescent dye that serves as a sensitive marker for zinc-rich granules [34]. Cells were then washed analysed by flow cytometry to identify those cells marked by both ZIGIR and the epithelial cell markers (Figure 5). The non-luminal epithelial cells displayed very little ZIGIR (0.05% of stromal cells and leukocytes; 0.48% of non-luminal epithelial cells) while the luminal epithelial cells were largely (12.7% of all cells) ZIGIR positive.

2.6 Glucose stimulated zinc secretion in cancerous cell lines

Our previous work with TRAMP mice demonstrated that GdL-1, a zinc responsive MRI contrast agent, could detect differential zinc secretion from the healthy prostate and prostate cancer only after glucose stimulation, suggesting the movement of intracellular zinc into the extracellular space [18]. To understand how this may apply to human-derived cancer cell lines, ZIMIR-based fluorescent experiments involving two prostate cancer cell lines, C4.2 (isolated from a human prostate cancer LNCaP cell subcutaneous xenograft tumour of castrated mouse) and PC3 (isolated from a bone metastasis of a grade IV prostatic adenocarcinoma), were undertaken [37]. Similar to our previous experiments, cells were cultured in a zinc-rich medium for 72 hours prior to confocal fluorescent imaging. Interestingly, the prostate cancer cell lines could not tolerate 150 μM $ZnSO_4$ so a reduced amount (75 μM) was added to the growth media. After growth to confluence, the culture medium was removed and the cells were exposed to 1 μM ZIMIR followed by imaging in the presence of low (3 mM) versus high (18 mM) glucose. PNT1A-WT cells were used as control. As shown in Figure 6, the background fluorescence signal from PNT1A cells was significantly higher ($p<0.05$) even before exposure to glucose and they released more Zn^{2+} after exposure to glucose compared to the two cancer cell lines. This is consistent with less storage of Zn^{2+} in the cancer cell lines. Nonetheless, addition of high glucose to the C4.2 and PC3 cells did stimulate release small but detectable amounts of Zn^{2+} from intracellular stores.

3. Discussion

The goal of this study was to determine which cellular pools of Zn^{2+} ions contribute to GSZS in prostate epithelial cells in response to an increase in glucose. Our results demonstrate that high glucose stimulates both efflux of Zn^{2+} ions via ZnT1 transporters and an increase in lysosomal storage of Zn^{2+} via ZnT4 transporters. While these results are in general similar to reports of zinc homeostasis in other cell lines [4, 6, 9], but there are some key differences. Increased lysosomal sequestration of Zn^{2+} in response to increased zinc supplementation in cell media has been demonstrated in HeLa cells and appears to be necessary to prevent zinc-induced cellular toxicity and apoptosis [9, 28]. Prostate cells use a similar mechanism to store excess Zn^{2+}. Exposure of PNT1A cells to high levels of $ZnSO_4$ in culture resulted in the appearance of lysosomal granules (Fig. 2) similar to that reported in other cell types [28]. The size and number of these lysosomal granules increased when the cells were also presented with higher levels of glucose. This feature, not reported in other cell types, may be unique to prostate cells (Fig. 4).

The disruption of lysosomal storage by treatment with Bafilomycin resulted in the appearance of much larger multi-vesicular bodies (MVBs) with only a small increase in cytosolic Zn^{2+} (Figs. 2 and 4). This is similar to that observed in recent studies of Bafilomycin treated HeLa cells [28] but the increase in cytosolic free Zn^{2+} was lower in PNT1A cells compared to HeLa cells despite a higher amount of $ZnSO_4$ in the cell culture media [28]. This suggests that PNT1A cells with a higher basal level of ZnT1 expression have an advantage in maintaining non-toxic levels of cytosolic Zn^{2+} even in the presence of excess $ZnSO_4$ in the culture medium. Given that MVBs are known to form exosomes for

secretion or conglomerate into lysosomes for intracellular storage [30], the excess MVBs seen here most likely reflect an additional defence mechanism to protect prostate cells against Zn^{2+} toxicity. A recent study demonstrated that ZnT1 forms heterodimers with other ZnT family members, and that these heterodimers can relocate to unexpected intracellular compartments in response to excess Zn^{2+} [29]. For example, ZnT1-ZnT2 heterodimers aggregated to lysosomes in HeLa cells, despite ZnT1 normally being found on the plasma membrane. In ZnT1-impared cells, even more MVBs are formed consistent with this being an extra defence mechanism. In ZnT4-impaired cells, the density of the zinc granules was substantially less (Fig. 2) consistent with the known role of ZnT4 in storage of intracellular Zn^{2+}.

Dynamic fluorescence imaging of shZnT1 cells demonstrated a near complete absence of Zn^{2+} efflux and a dramatic increase in cytosolic Zn^{2+} levels after glucose was increased from 3 to 18 mM (Fig. 3). It was recently reported that ZnT1 not only plays a role in Zn^{2+} efflux but also acts as a modulator of L-type calcium channel (LTCC) activity, a major Zn^{2+} and Ca^{2+} entry pathway [36]. Thus, the loss of ZnT1 activity in shZnT1 cells could impact both Zn^{2+} efflux and Zn^{2+} influx. Numerous studies have demonstrated ubiquitous expression of ZnT1 in the prostate and throughout human secretory tissues, including breast and pancreas [1, 4, 10, 11]. Of the eight known members of the ZnT transport family, only ZnT1 is known to reside predominantly on the plasma membrane. Thus, it was not surprising to find that ZnT1 plays a crucial role in GSZS. Furthermore, in cells where lysosomes were impaired by pre-treatment with Bafilomycin and, in addition, the level of ZnT1 was reduced, cytosolic zinc dramatically increased (Fig. 1J). Previous studies in HeLa cells and pancreatic cells have demonstrated zinc efflux via lysosomal exocytosis [28, 29, 30]. While we cannot completely rule out exocytosis of lysosomal Zn^{2+} contributing to GSZS in PNT1A cells, the near complete lack of GSZS in shZnT1 cells suggests the lysosomal contribution is small.

While the molecular mechanism of GSZS in prostate cells will require further studies, the current observations do offer some insights. It has long been known that Zn^{2+} inhibits aconitase-2 catalysed conversion of citrate to isocitrate resulting in accumulation of citrate [1, 2, 3]. The data presented here demonstrates that not only does glucose stimulate efflux of Zn^{2+} from cells but also increases cytosolic Zn^{2+} (Fig. 3a). The intracellular distribution of Zn^{2+} in prostate epithelia cells is reportedly ~70% in the nucleus, 24% in the mitochondria, and 6% in the cytosol [27]. If one considers the possibility that the mobile pool contributing to the increase in cytosolic Zn^{2+} could originate from the mitochondrial component, this would lower inhibition of aconitase-2 and thereby allow increased oxidative flux through TCA cycle. This would provide an elegant mechanism for connecting the balance between mitochondrial levels of Zn^{2+} with glucose oxidation but this study did not directly test that hypothesis.

In human prostate tissue, we show here that luminal epithelial cells are the only cell type that contain high levels of zinc granules (Fig. 5). We previously demonstrated in mouse prostate that there are dramatic differences in GSZS between healthy prostate and prostate carcinoma [18]. The new observation here that luminal epithelial cells isolated from surgically removed human BPH tissue contain the most Zn^{2+} suggests that the GSZS

response detected by MRI likely originates from luminal epithelial cells. Whether prostate cancer originates in the basal epithelial or luminal epithelial cells remains an open question [35] but the presence of zinc granules in luminal epithelial cells from human BPH samples suggests that GSZS is preserved in BPH nodules and that zinc-responsive MRI contrast agents may be able to detect differential Zn^{2+} secretion between nascent prostate cancer and BPH nodules in the human prostate. Interestingly, while a decrease in total Zn^{2+} was observed in both the C4.2 and PC3 prostate cancer cell lines compared to PNT1A-WT cells, GSZS did occur to some extent in all three cell types. The decrease in total cellular Zn^{2+} in prostate cancer compared to normal prostate tissue is well known but, to our knowledge, no one has previously examined whether GSZS also occurs prostate cancer cells before this study. Whether the decrease in Zn^{2+} excretion between cancerous cells and wild-type cells represents a clinically significant difference that could possibly be detected *in vivo* using a zinc-responsive MRI probe. If successful, this would represent a breakthrough in the use of MRI for unequivocal diagnosis of prostate cancer.

Decreased expression of ZIP1, down-regulation of ZnT4, and a decrease in total cellular Zn^{2+} are all characteristic features of prostate carcinoma (PCa) [12,13]. Given the current observation that glucose stimulates both export and storage of Zn^{2+} in the healthy prostate cells, one could reasonably ask whether there is a correlation between prolonged hyperglycaemia and the incidence of PCa. Although male diabetic patients do have a higher risk of developing benign prostatic hyperplasia (BPH) and typically have more severe symptoms from BPH than non-diabetics [23, 24, 25], the risk of developing PCa is surprisingly slightly lower in men with type II diabetes[24]. Given that total tissue Zn^{2+} is reportedly higher in BPH tissue than in normal healthy prostate [26] and the origins of human BPH (transition zone) and PCa (peripheral zone) differ in the prostate, the epithelial cells from these two tissue regions may respond differently to chronic hyperglycaemia [7]. Thus, further studies will be needed to evaluate the redistribution of zinc transporters in BPH tissue, prostatic intraepithelial neoplasia (PIN), and prostate cancer in order to understand the role of glucose and potentially other extracellular stimuli in modulating Zn^{2+} homeostasis.

Materials and methods

Cell culture

The prostatic epithelial cell line, PNT1A-WT, was kindly provided by Dr. JT Hsieh at UT Southwestern Medical Center at Dallas and maintained in RPMI-1640 medium (Sigma, R81508) supplemented with 10% of fetal bovine serum (Atlanta Biologicals, S11195) and 20 units of Penicillin-Streptomycin (Life Technologies, 15140–122). For the cells with zinc supplementation, $ZnSO_4$ (Sigma, Z2876) at various concentrations (75, 150, and 300 μM) and glucose (Sigma, G8644) were added directly to the glucose-free RPMI-1640 medium (Gibco, 11879).

Confocal fluorescence imaging for zinc distribution and release using Zn-sensing probes

For the confocal imaging, 5×10^5 cells were cultured in 35-mm^2 Petri imaging dishes with glass bottoms (MatTek, P35G-0–10-C) with or without supplement of $ZnSO_4$ (150 μM for

general experiments of PNT1A and 75 μM for prostate cancer cell lines) in RPMI-1640 culture medium with basal level of glucose (6 mM) for 24 hrs. After 24 hr incubation, culture medium was removed and the cells were washed with a secretion assay buffer (SAB) containing 114 mM NaCl, 4.7 mM KCl, 1.2 mM KH_2PO_4, 2.5 mM $CaCl_2$, 1.16 mM $MgSO_4$, 3 mM glucose, and 20 mM HEPES (pH 7.4). The cell permeable zinc sensor, FluoZin-1-AM (Thermo), was used to detect the intracellular zinc distribution. In addition, the zinc release was detected by a cell membrane bound zinc sensor (ZIMIR) which was provided by Dr. Wen-hong Li at UT Southwestern Medical Center at Dallas). LysoTracker® Red DND-99 was used to label lysosomes by incubating the cells for 30 min at room temperature. FluoZin-1-AM was prepared for intracellular Zn(II) measurement by reconstruction with 20% Pluronic F-127 (Thermo)(1 : 2 ratio) within final concentration of 50 ng/μl in SAB and loaded to the cells for 30 min at room temperature or 37°C, respectively. ZIMIR was prepared in SAB for a final concentration of 1 μM with supplementation of 1 μM EDTA and loaded into the cell medium for 15 min at room temperature. After loading the zinc sensors, the cells were rinsed twice with SAB, incubated at room temperature, and imaged using an inverted Zeiss LSM 780 multi-photon laser scanning confocal microscope. Images were analysed by Image J and the data was presented as mean ± SEM of integrated fluorescence intensity from 8 individual cells of three separate experiments. Regions of interest (ROIs) were drawn around clusters of cells in the PNT1A-shZnT1, PNT1A-shZnT4, and PNT1A-WT cell lines; data was presented as a mean ± SEM of integrated fluorescence intensity from 8 individual cells of a single experiment in the C4–2 and PC-3 cell lines.. Unpaired *t*-test was used for statistical analysis.

Lentivirus-mediated generation of PNT1A cells with knockdown of ZnT1 and ZnT4

Stable cells with decreased expression of ZnT1 (SLC30A1) and ZnT4 (SLC30A4) were generated by lentivirus-mediated shRNA expression. The pLKO.1-Puro vector expressing shRNA sequences targeting ZnT1 (target sequence of 3 clones: CCTGCAAAGCATTTGTAGAAA, GCTACTACCATTCAGCCTGAA, and GAAGTACAAGTGAATGGAAAT), and ZnT4 (target sequence of 3 clones: CATACGATTCAAGCCAGAATA, CATAGTTCACATACAGCTAAT, and TATGGGATACAGTAGTTATAA) were obtained from OpenBiosystems, and viruses were generated at the Department of Urology of the UT Southwestern Medical Center. Polyclonal pooled populations of stable cells were selected in the presence of puromycin (2 μg/ml) for more than 3 passages before initiating any functional experiments. Western blot was performed for evaluate the knockdown efficiency of shZnT1 and shZnT4 (Figure S1).

Transmission Electron Microscopy

Cells were fixed with 2.5% (v/v) glutaraldehyde in 0.1M sodium cacodylate buffer (pH7.4) in the culture dish (150 mm^2). After 10 min of fixation, cells were released from the plastic dishes by gentle scraping, pelleted with glass pipet and kept in fixation solution at 4°C overnight. After three rinses with 0.1M sodium cacodylate buffer, cell pellets were embedded in 3% agarose and sliced into 1 mm^3 blocks, rinsed with the same buffer three times and post-fixed with 1% osmium tetroxide and 0.8% potassium ferricyanide in 0.1M sodium cacodylate buffer for 1.5 hr at room temperature. Cells were then rinsed with water and en-bloc stained with 4% uranyl acetate in 50% ethanol for 2 hr. Cells were dehydrated

with increasing concentration of ethanol, transitioned into propylene oxide, infiltrated with Embed-812 resin and polymerized in a 60°C oven overnight. Blocks were sectioned with a diamond knife (Diatome) on a Leica Ultracut 6 ultramicrotome (Leica Microsystems) and collected onto copper grids, post stained with 2% aqueous uranyl acetate and lead citrate. Images were acquired on a Tecnai G2 spirit transmission electron microscope (FEI) equipped with a LaB6 source using a voltage of 120 kV.

Flow cytometry assessment of BPH ZIGIR uptake

BPH specimens were obtained fresh from patients undergoing simple prostatectomy at UT Southwestern Medical Center. Fresh tissue samples were transported in ice-cold saline and digested into single cells as described previously (1). Digested cells were pelleted and stained as described previously (2, 3). The following antibodies were used against cell surface markers: CD326 (Biolegend 324226), CD26 (Biolegend 302704). Following antibody staining, cells were washed with DPBS (1.5 mL x 2 times) and then with a secretion assay buffer (SAB) containing 114 mM NaCl, 4.7 mM KCl, 1.2 mM KH_2PO_4, 2.5 mM $CaCl_2$, 1.16 mM $MgSO_4$, 3 mM glucose, and 20 mM Hepes (pH 7.4). Cells were then incubated with ZIGIR (1.0 μM) in SAB at 37 °C for 15 min and washed with cell sorting buffer before analysis. Stained cells were analyzed at the UT Southwestern CRI Flow Cytometry Core on a BD FACSAria FUSION SORP 5-laser flow cytometer and analyzed with FlowJo software.

Supplementary Material

Refer to Web version on PubMed Central for supplementary material.

Acknowledgements

We thank Dr. Wen-hong Li (Department of Cell Biology, UT Southwestern Medical Center) for the gift of the ZIMIR and critical reading of the manuscript. This work was supported by grants from the National Institutes of Health (R01-DK095416), the Robert A. Welch Foundation (AT-584), and the Cancer Prevention & Research Institute of Texas (RP-180178).

References

1. Costello LC, et al. “Mitochondrial Function, Zinc, and Intermediary Metabolism Relationships in Normal Prostate and Prostate Cancer.” Mitochondrion, vol. 5, no. 3, 6 2005, pp. 143–53., doi:10.1016/j.mito.2005.02.001. [PubMed: 16050980]
2. Kavanagh JP “Isocitric and Citric Acid in Human Prostatic and Seminal Fluid: Implications for Prostatic Metabolism and Secretion.” The Prostate, vol. 24, no. 3, 1994, pp. 139–42. [PubMed: 8115279]
3. Singh Keshav K., et al. “Mitochondrial Aconitase and Citrate Metabolism in Malignant and Nonmalignant Human Prostate Tissues.” Molecular Cancer, vol. 5, Apr. 2006, p. 14., doi:10.1186/1476-4598-5-14. [PubMed: 16595004]
4. Kelleher Shannon L., et al. “Zinc in Specialized Secretory Tissues: Roles in the Pancreas, Prostate, and Mammary Gland.” Advances in Nutrition (Bethesda, Md.), vol. 2, no. 2, Mar. 2011, pp. 101–11., doi:10.3945/an.110.000232.
5. Costello LC, and Franklin RB. “Novel Role of Zinc in the Regulation of Prostate Citrate Metabolism and Its Implications in Prostate Cancer.” The Prostate, vol. 35, no. 4, June 1998, pp. 285–96. [PubMed: 9609552]

6. Franklin Renty B., et al. “Zinc and zinc transporters in normal prostate function and the pathogenesis of prostate cancer”, Frontiers in Bioscience : A Journal and Virtual Library, 2005, 10: 2230–39. [PubMed: 15970489]
7. Verze Paolo, et al. “The Role of the Prostate in Male Fertility, Health and Disease.” Nature Reviews Urology, vol. 13, no. 7, July 2016, pp. 379–86. www.nature.com, doi:10.1038/nrurol.2016.89. [PubMed: 27245504]
8. Jayaraman Arathi K., and Jayaraman Sundararajan. “Increased Level of Exogenous Zinc Induces Cytotoxicity and Up-Regulates the Expression of the ZnT-1 Zinc Transporter Gene in Pancreatic Cancer Cells.” The Journal of Nutritional Biochemistry, vol. 22, no. 1, Jan. 2011, pp. 79–88., doi:10.1016/j.jnutbio.2009.12.001. [PubMed: 20392624]
9. Kukic Ira, et al. “Zn^{2+} Efflux through Lysosomal Exocytosis Prevents Zn^{2+}-Induced Toxicity.” J. Cell Sci, 2014, 127:3094–103., doi:10.1242/jcs.145318. [PubMed: 24829149]
10. Takagishi Teruhisa, et al. “Recent Advances in the Role of SLC39A/ZIP Zinc Transporters In Vivo.” Int. J. Mol. Sci, 2017, p. 21.
11. Franklin RB, et al. “Human ZIP1 Is a Major Zinc Uptake Transporter for the Accumulation of Zinc in Prostate Cells.” J. Inorg. Biochem, 2003, 96: 435–42. [PubMed: 12888280]
12. Franklin Renty B., et al. “HZIP1 Zinc Uptake Transporter down Regulation and Zinc Depletion in Prostate Cancer.” Molecular Cancer, vol. 4, Sept. 2005, p. 32., doi:10.1186/1476-4598-4-32. [PubMed: 16153295]
13. Beck Frances W. J., et al. “Differential Expression of HZnT-4 in Human Prostate Tissues.” The Prostate, vol. 58, no. 4, 2004, pp. 374–81. Wiley Online Library, doi:10.1002/pros.10344. [PubMed: 14968438]
14. Palmiter Richard D. “Protection against Zinc Toxicity by Metallothionein and Zinc Transporter 1.” Proc. National Acad. Sci. USA, 2004, 101: 4918–23. doi:10.1073/pnas.0401022101.
15. Sankavaram Kavitha, and Freake Hedley C.. “The Effects of Transformation and ZnT-1 Silencing on Zinc Homeostasis in Cultured Cells.” The Journal of Nutritional Biochemistry, vol. 23, no. 6, June 2012, pp. 629–34., doi:10.1016/j.jnutbio.2011.03.006. [PubMed: 21775119]
16. Kolenko Vladimir, et al. “Zinc and Zinc Transporters in Prostate Carcinogenesis.” Nature Reviews. Urology, vol. 10, no. 4, Apr. 2013, pp. 219–26., doi:10.1038/nrurol.2013.43. [PubMed: 23478540]
17. Henshall Susan M., et al. “Expression of the Zinc Transporter ZnT4 Is Decreased in the Progression from Early Prostate Disease to Invasive Prostate Cancer.” Oncogene, vol. 22, no. 38, Sept. 2003, pp. 6005–12., doi:10.1038/sj.onc.1206797. [PubMed: 12955079]
18. Clavijo Jordan, Veronica M, et al. “Zinc-Sensitive MRI Contrast Agent Detects Differential Release of Zn(II) Ions from the Healthy vs. Malignant Mouse Prostate.” Proceedings of the National Academy of Sciences of the United States of America, vol. 113, no. 37, 13 2016, pp. E5464–5471., doi:10.1073/pnas.1609450113. [PubMed: 27562169]
19. Mauvezin Caroline, and Neufeld Thomas P.. “Bafilomycin A1 Disrupts Autophagic Flux by Inhibiting Both V-ATPase-Dependent Acidification and Ca-P60A/SERCA-Dependent Autophagosome-Lysosome Fusion.” Autophagy, vol. 11, no. 8, Sept. 2015, pp. 1437–38. PubMed Central, doi:10.1080/15548627.2015.1066957. [PubMed: 26156798]
20. Shin H, et al., “The Formation of Multivesicular Bodies in Activated Blastocysts Is Influenced by Autophagy and FGF Signaling in Mice”, Sci. Reports, 2017, 7:41986. doi: 10.1038/srep41986.
21. Kanemoto Soshi, et al. “Multivesicular Body Formation Enhancement and Exosome Release during Endoplasmic Reticulum Stress.” Biochemical and Biophysical Research Communications, vol. 480, no. 2, 11 2016, pp. 166–72., doi:10.1016/j.bbrc.2016.10.019. [PubMed: 27725157]
22. Li Daliang, et al. “Imaging Dynamic Insulin Release Using a Fluorescent Zinc Indicator for Monitoring Induced Exocytotic Release (ZIMIR).” Proceedings of the National Academy of Sciences of the United States of America, vol. 108, no. 52, Dec. 2011, pp. 21063–68., doi:10.1073/pnas.1109773109. [PubMed: 22160693]
23. Waters Kevin M., et al. “No Association of Type-2 Diabetes Risk Variants and Prostate Cancer Risk: The Multiethnic Cohort and PAGE.” Cancer Epidemiology, Biomarkers & Prevention : A Publication of the American Association for Cancer Research, Cosponsored by the American Society of Preventive Oncology, vol. 20, no. 9, Sept. 2011, pp. 1979–81. PubMed Central, doi:10.1158/1055-9965.EPI-11-0019.

24. Waters Kevin M., et al. “Association of Diabetes With Prostate Cancer Risk in the Multiethnic Cohort.” American Journal of Epidemiology, vol. 169, no. 8, Apr. 2009, pp. 937–45. PubMed Central, doi:10.1093/aje/kwp003. [PubMed: 19240222]
25. Breyer Benjamin N., and Sarma Aruna V.. “Hyperglycemia and Insulin Resistance and the Risk of BPH/LUTS: An Update of Recent Literature.” Current Urology Reports, vol. 15, no. 12, Dec. 2014, p. 462. PubMed Central, doi:10.1007/s11934-014-0462-x. [PubMed: 25287259]
26. Sapota Andrzej, et al. “Disturbed Homeostasis of Zinc and Other Essential Elements in the Prostate Gland Dependent on the Character of Pathological Lesions.” BioMetals, vol. 22, no. 6, July 2009, p. 1041. Springer Link, doi:10.1007/s10534-009-9255-y. [PubMed: 19629715]
27. Tvedt KE, Kopstad G, Haugen OA, and Halgunset J. “Subcellular Concentrations of Calcium, Zinc, and Magnesium in Benign Nodular Hyperplasia of the Human Prostate: X-Ray Microanalysis of Freeze-Dried Cryosections.” INTRACELLULAR CALCIUM, n.d., 7.
28. Kukic Ira, Lee Jeffrey K., Coblentz Jessica, Kelleher Shannon L., and Kiselyov Kirill. “Zinc-Dependent Lysosomal Enlargement in TRPML1-Deficient Cells Involves MTF-1 Transcription Factor and ZnT4 (Slc30a4) Transporter.” The Biochemical Journal 451, no. 2 (April 15, 2013): 155–63. 10.1042/BJ20121506. [PubMed: 23368743]
29. Kukic Ira, Lee Jeffrey K., Coblentz Jessica, Kelleher Shannon L., and Kiselyov Kirill. “Zinc-Dependent Lysosomal Enlargement in TRPML1-Deficient Cells Involves MTF-1 Transcription Factor and ZnT4 (Slc30a4) Transporter.” The Biochemical Journal 451, no. 2 (April 15, 2013): 155–63. 10.1042/BJ20121506. [PubMed: 23368743]
30. Soekmadji Carolina, Russell Pamela J., and Nelson Colleen C.. “Exosomes in Prostate Cancer: Putting Together the Pieces of a Puzzle.” Cancers 5, no. 4 (December 2013): 1522–44. 10.3390/cancers5041522. [PubMed: 24351670]
31. Joseph Diya B., Henry Gervaise H., Malewska Alicia, Iqbal Nida S., Ruetten Hannah M., Turco Anne E., Abler Lisa L., et al. “Urethral Luminal Epithelia Are Castration-Insensitive Progenitors of the Proximal Prostate.” Preprint. Cell Biology, February 19, 2020. 10.1101/2020.02.19.937615.
32. Henry Gervaise H., Loof Nicolas, and Strand Douglas W.. “OMIP-040: Optimized Gating of Human Prostate Cellular Subpopulations.” Cytometry. Part A : The Journal of the International Society for Analytical Cytology 91, no. 12 (December 2017): 1147–49. 10.1002/cyto.a.23187. [PubMed: 28834328]
33. Strand Douglas W., Costa Daniel N., Francis Franto, Ricke William A., and Roehrborn Claus G.. “Targeting Phenotypic Heterogeneity in Benign Prostatic Hyperplasia.” Differentiation; Research in Biological Diversity 96 (2017): 49–61. 10.1016/j.diff.2017.07.005 [PubMed: 28800482]
34. Zadeh, Ghazvini Ebrahim H, Huang ZhiJiang, Xia Jing, Li Daliang, Davidson Howard W, Li Wen-hong, “ZIGIR, a Granule-Specific Zn^{2+} Indicator, Reveals Human Islet a Cell Heterogeneity”, Cell Reports (2020); 10.1016/j.celrep.2020.107904
35. Xin L “Cells of Origin for Cancer: An Updated View from Prostate Cancer.” Oncogene 32, no. 32 (August 8, 2013): 3655–63. 10.1038/onc.2012.541. [PubMed: 23178496]
36. Shusterman Eden, Beharier Ofer, Levy Shiri, Zarivach Raz, Etzion Yoram, Campbell Craig R., Lee Il-Ha, et al. “Zinc Transport and the Inhibition of the L-Type Calcium Channel Are Two Separable Functions of ZnT-1.” Metallomics 9, no. 3 (March 22, 2017): 228–38. 10.1039/C6MT00296J. [PubMed: 28091657]
37. Cunningham David, and You Zongbing. “In Vitro and in Vivo Model Systems Used in Prostate Cancer Research.” Journal of Biological Methods 2, no. 1 (2015). 10.14440/jbm.2015.63.

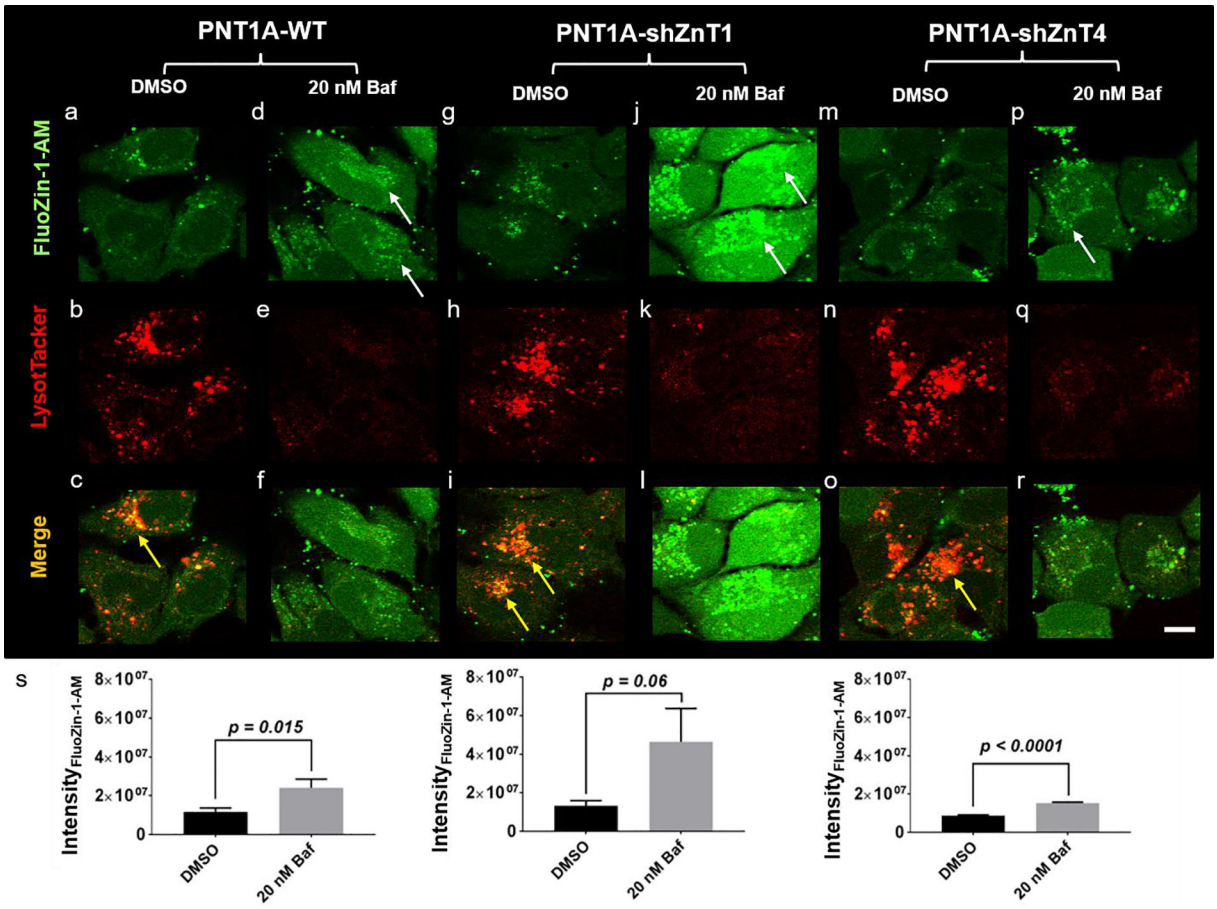

Figure 1:

(a-f) Confocal images of PNT1A-WT, **(g-l)** PNT1A-shZnT1, and **(m-r)** PNT1A-shZnT4 treated overnight with 150 μM $ZnSO_4$ and 20 nM Baf or DMSO, then loaded with zinc-responsive probe, FluoZin-1-AM (green) plus LysoTracker (red). **(c, i, and o**) FluoZin-1-AM and LysoTracker co-localize in the cells not treated with Baf (yellow). **(e, k, and q)** The LysoTracker fluorescence signal disappears in cells treated with Baf treatment**. (d, j, and p)** The FluoZin-1-AM signal localizes in granules in all cells lacking lysosomes (Baf-treated) (white arrows). **(j)** In PNT1A-shZnT1 cells treated with Baf, a strong FluoZin-1-AM signal appears in the cytosol and in granules. **(s)** Quantitative fluorescence signal intensity of FluoZin-1-AM for each condition is displayed. These studies were carried out using a Zeiss 780 inverted confocal laser scanning microscope (CLSM). Scale bar = 10 μm. Triplicate sample for each condition.

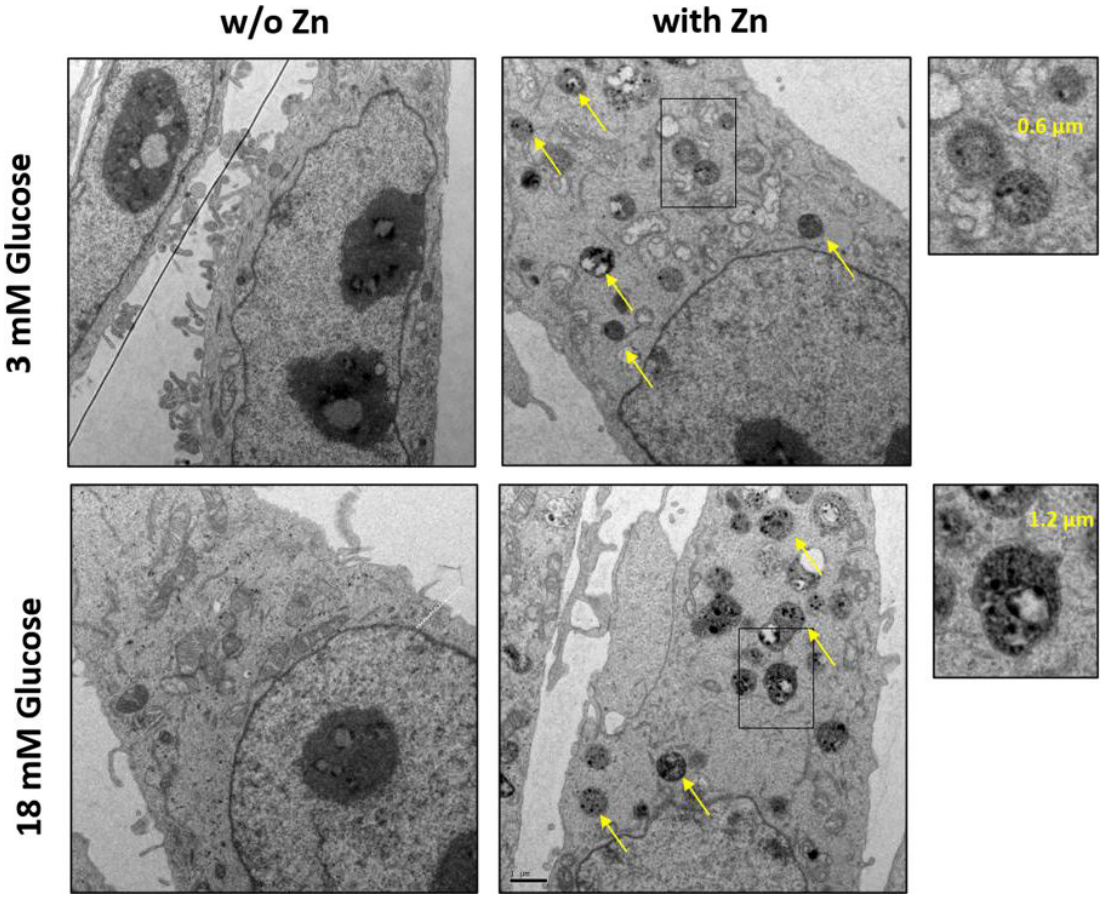

Figure 2:

Electron micrographs of a PNT1A-WT cells cultured for 72 hours with or without $ZnSO_4$ (300 µM), then challenged with either low (3 mM) or high (18 mM) glucose for 15 minutes. Large storage lysosomes are marked with yellow arrows. Duplicate for each condition.

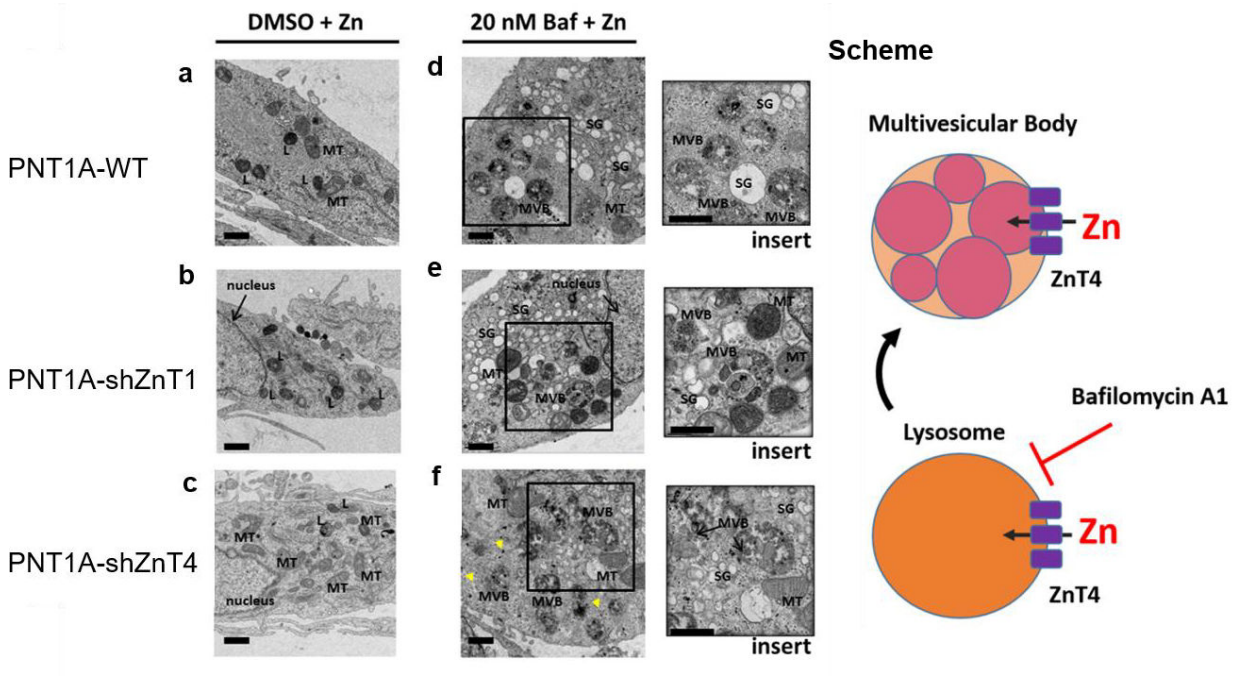

Figure 3:

(a and b) Electron micrograph of PNT1A-WT, **(c and d)** PNT1A-shZnT1, and **(e and f)** PNT1A-shZnT4 cells without or with treatment of 20 nM Baf. Cells were incubated with 150 μM $ZnSO_4$ for 24 hrs. **(f)** Yellow arrow heads indicate condensed cytosolic zinc. Scale bar = 1 μm. MT: mitochondria, L: lysosome, SG: secretory granule, MVB: multi-vesicular body. Triplicate sample for each condition.

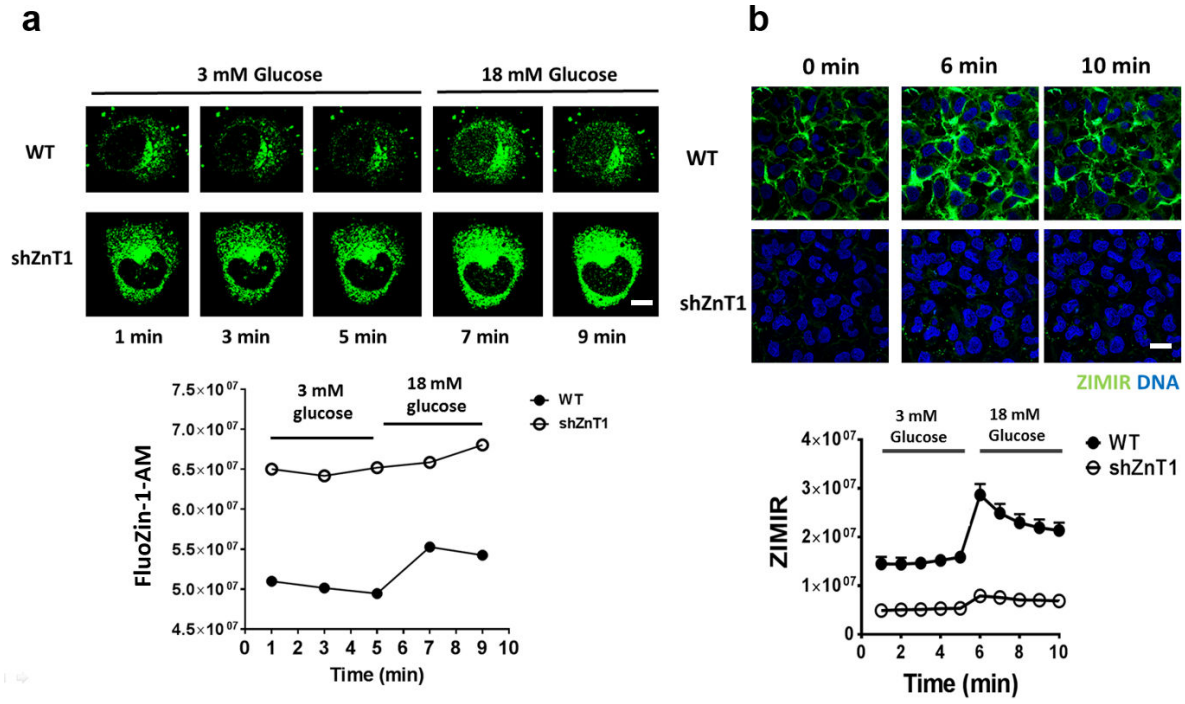

Figure 4:

(a) Intracellular zinc imaging using an intracellular zinc probe, FluoZin-1-AM, on PNT1A-WT and zinc efflux impaired (PNT1A-shZnT1) cells. The glucose concentration was changed from 3 to 18 mM after 5 mins of imaging (arrow). The lower graph (left) shows the FluoZin-1AM signal intensity during the live cell imaging. Scale bar = 10 μm. **(b)** *In vitro* confocal images of glucose-stimulated zinc secretion in PNT1A-WT and PNT1A-shZnT1 cells using the membrane-bound zinc responsive fluorescence probe ZIMIR (green). DAPI was used for nuclear staining (blue). Cells were treated with 150 μM $ZnSO_4$ for 72 hr prior to imaging and challenged with 3 mM glucose (at 0 min) and then 18 mM glucose (at 5 min). Zn^{2+} export was quantified by monitoring ZIMIR fluorescence. Both experiments were carried out on a Zeiss 780 inverted confocal laser-scanning microscope (CLSM). Scale bar = 20 μm. Triplicate sample for each condition.

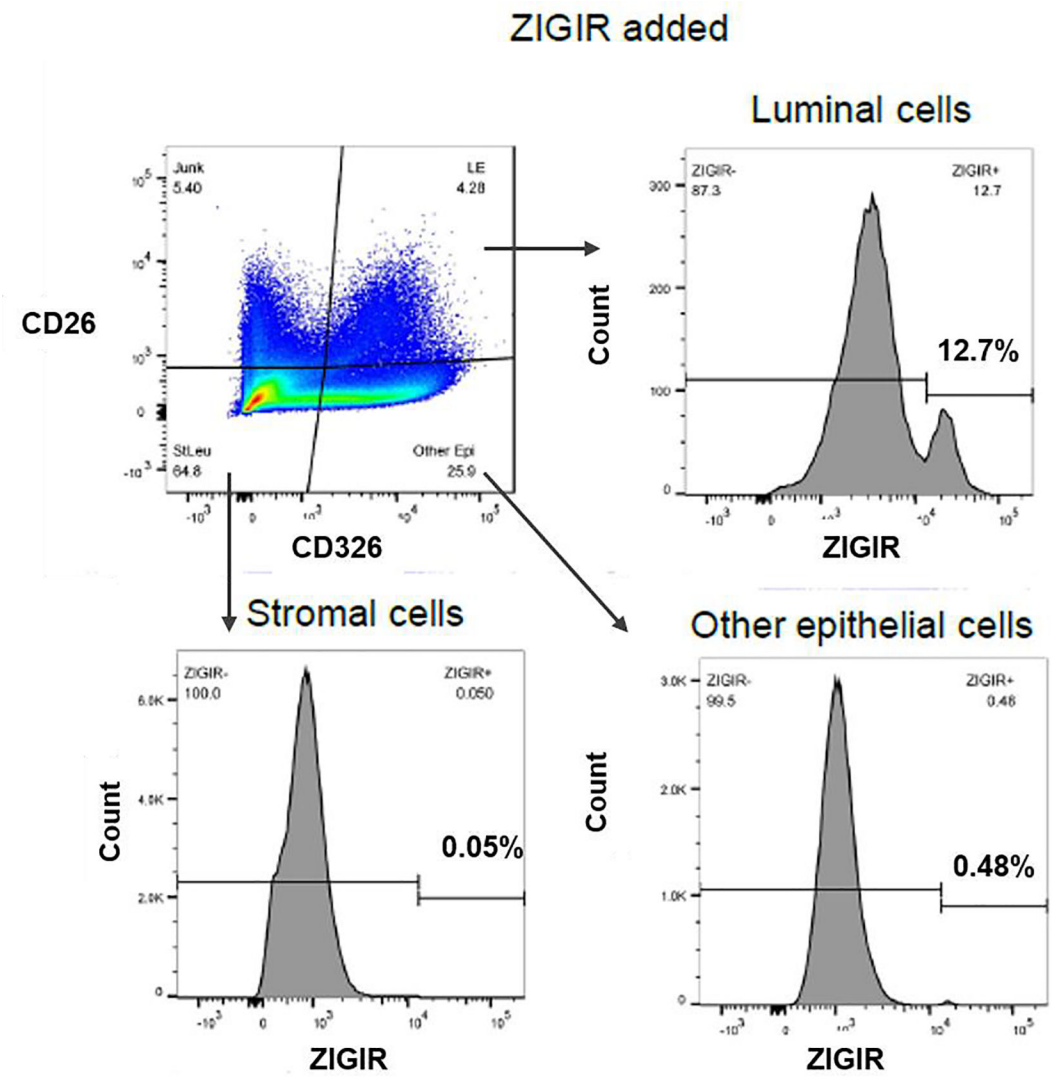

Figure 5:

Flow cytometry analysis of isolated human prostate BPH cells after exposure to ZIGIR to mark zinc-rich granules. The luminal cells were the only cell type that displayed a ZIGIR positive signal, indicating the presence of intracellular zinc granules.

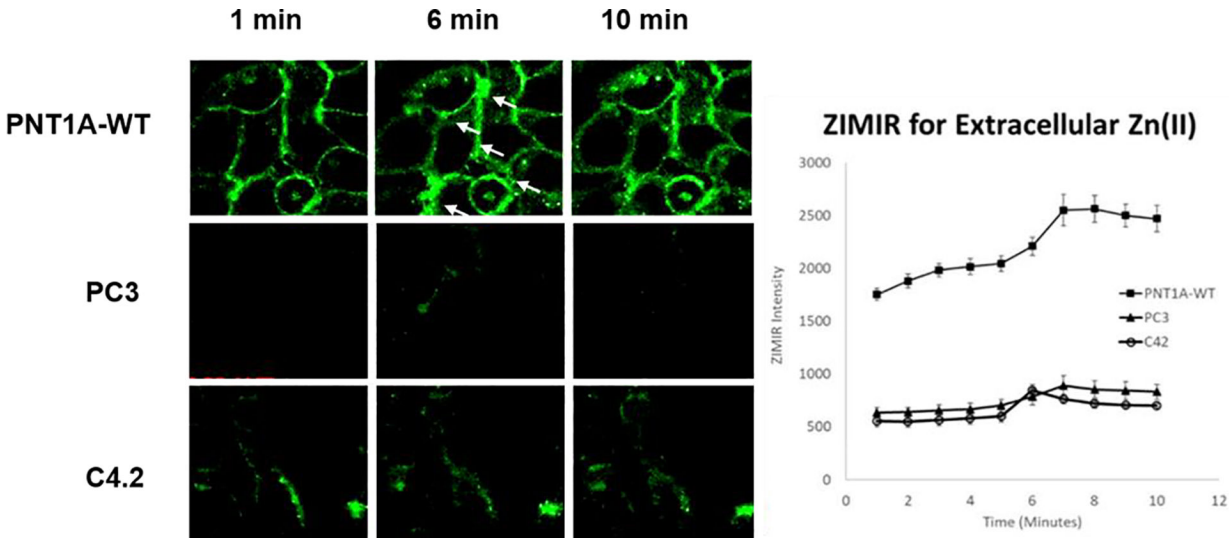

Figure 6:

In vitro confocal images of glucose-stimulated zinc secretion in PNT1A-WT, PC3, and C4.2 cells using the membrane-bound zinc-responsive fluorescence probe ZIMIR. Cells were treated with 75 μM $ZnSO_4$ for 72 hr prior to imaging and challenged with 3 mM glucose (at 0 min) and then 18 mM glucose (at 5 min). Zn^{2+} export was quantified by monitoring ZIMIR fluorescence. Both experiments were carried out on a Zeiss 780 inverted confocal laser-scanning microscope (CLSM). Duplicate for each condition.